Forward-angle neutron-proton scattering at 96 MeV

C. Johansson,[1] J. Blomgren,[1,*] A. Ataç,[1] B. Bergenwall,[1] S. Dangtip,[1,2] K. Elmgren,[3] A. Hildebrand,[1] O. Jonsson,[4] J. Klug,[1]
P. Mermod,[1] P. Nadel-Turonski,[5,6] L. Nilsson,[1,4] N. Olsson,[1,3] S. Pomp,[1] A. V. Prokofiev,[4] P.-U. Renberg,[4]
U. Tippawan,[1,2] and M. Österlund[1]

[1]*Department of Neutron Research, Uppsala University, Box 525, S-75120 Uppsala, Sweden*
[2]*Department of Physics, Chiang Mai University, Thailand*
[3]*Swedish Defence Research Agency (FOI), Stockholm, Sweden*
[4]*Svedberg Laboratory, Uppsala University, Sweden*
[5]*Department of Radiation Sciences, Uppsala University, Sweden*
[6]*George Washington University, Washington, D.C., USA*

The differential np scattering cross section has been measured at 96 MeV in the angular range $\theta_{\mathrm{c.m.}} = 20°–76°$.
Together with an earlier data set at the same energy, covering the angles $\theta_{\mathrm{c.m.}} = 74°–180°$, a new data set has been
formed in the angular range $\theta_{\mathrm{c.m.}} = 20°–180°$. This extended data set has been normalized to the experimental
total np cross section, resulting in a renormalization of the earlier data of 0.7%, which is well within the reported
normalization uncertainty for that experiment. A novel normalization technique has been investigated. The results
on forward np scattering are in reasonable agreement with theory models and partial wave analyses and have
been compared with data from the literature.

I. INTRODUCTION

The neutron-proton scattering cross section plays an important role in fundamental physics, since it can be used to derive a value of the absolute strength of the strong interaction between nucleons, i.e., the pion-nucleon coupling constant, $g_{\pi NN}^2$. The πNN coupling constant governs the properties of the two-nucleon system to such an extent that only a few percent difference in its value is sufficient to either unbind the deuteron or to produce a bound diproton, in both cases with major cosmological consequences. Moreover, its precise value is of crucial importance for the quantitative discussion of a large number of phenomena in hadron and nuclear physics.

The actual value of the πNN coupling constant is quoted at the pion pole, where the square of the momentum transfer q^2 is equal to $-m_\pi^2$, where m_π is the pion mass. It is therefore not directly available from experimental data, but at $180°$ np scattering, the conditions are close to this limit. As a consequence, backward np scattering data have often been used to extract the charged coupling constant, $g_{\pi^\pm NN}^2$. In such determinations, both the absolute normalization and the shape of the angular distribution close to $180°$ are of importance for the extracted value of $g_{\pi NN}^2$.

Unfortunately, there are severe discrepancies in the differential np scattering cross section database in the energy region 100–1000 MeV [1]. It is dominated by two large data sets, one from Los Alamos National Laboratory (LANL) (Bonner *et al.* [2], Evans *et al.* [3,4], Jain *et al.* [5], and Northcliffe *et al.* [6]) and the other from Paul Scherrer Institute (PSI) (Hürster *et al.* [7], recently replaced by Franz *et al.* [8]). Until recently, the LANL data constituted almost 50% of the database. The

recent publication of an extended PSI data set [8] means that these data now account for over 60% of the statistical weight of the database.

The two data sets are incompatible when only statistical uncertainties are considered. Above about 500 MeV, the angular distribution shapes of these two sets agree reasonably well, while at 200 MeV, the $150°/180°$ cross section ratios differ by as much as 10–15%. Unfortunately, the systematic uncertainties are not well known for the two data sets. It cannot be excluded that at least part of the discrepancy is related to systematic effects not taken into account [9].

These two large data sets can serve to illustrate the incompatibility problems, but these difficulties are not unique. A large number of other experiments also differ significantly. It has been concluded that the np scattering cross section is known to only about 10%, using experimental information only [1].

Besides shape differences, there also seem to be inconsistencies in the normalization of np data, which is not surprising, because absolute measurements of neutron beam intensities are notoriously difficult [10]. This is because the only way to determine the number of neutrons in a beam is to detect charged particles produced in neutron-induced nuclear reactions; but to measure the cross section for those reactions, the beam intensity has to be known.

There are ways to circumvent this dilemma, but they are associated with painstaking efforts. Below the pion-production threshold at about 270 MeV, two methods have been used to determine the np scattering cross section absolutely. One of the methods is tagging, i.e., neutrons are produced in a nuclear reaction where the detection of associated charged particles gives unambiguous information about the neutron. For instance, at low energies, the ^{2}H(d,^{3}He)n reaction has

*Corresponding author, Tel. +46 18 471 3788, email address: jan.blomgren@tsl.uu.se.

been used in measurements where determination of the energy and direction of the ^{3}He recoil gives information about the neutron energy and direction, and the mere presence of the ^{3}He recoil implies that a neutron has been produced. Thereby, this technique can be used to produce neutron beams of low, but well-known, intensity.

The second method is to combine a relative measurement of the *np* angular distribution with information about the total *np* cross section. The total cross section can be determined without knowledge of the absolute beam intensity; a measurement of the relative beam attenuation in a target is sufficient, and therefore total cross sections are often known to about 1%. Below the pion-production threshold, the inelastic channels in *np* interactions, i. e., capture and bremsstrahlung, are very weak and contribute far less than 1% to the total cross section. Thus, the total and differential *np* cross sections are directly linked via the relation

$$\sigma_T = \int \frac{d\sigma}{d\Omega} d\Omega = \int_{0°}^{180°} 2\pi \, \sin(\theta) \frac{d\sigma(\theta)}{d\Omega} d\theta. \tag{1}$$

Previously, our group studied *np* scattering in the backward angular range. At 96 MeV, data in the 74°–180° angular range have been published [11]. Since part of the total angular range was missing, the normalization was obtained in a procedure where the undetected fraction of the angular distribution was obtained from partial wave analyses and *NN* interaction models. This has motivated us to conduct the present experiment on forward-angle *np* scattering. Extending the angular distribution to cover 20°−180° allows a purely experimental normalization. The missing part (0°−20°) gives very small contributions to the uncertainty in the normalization, because the solid angle vanishes at zero degrees.

Recently, a novel technique for normalization of neutron-induced cross sections has been presented [12]. In elastic neutron scattering from nuclei, the absolute scale can be provided with a method similar to the one of Eq. (1), with the difference that a relative angular distribution of elastic scattering is normalized to the total elastic cross section. The latter, in turn, can be derived from the difference between the total cross section and the reaction cross section. In a recent experiment on elastic neutron scattering from ^{12}C and ^{208}Pb, this technique was found to have an uncertainty of 3%. Thereby, a measurement of the ^{12}C/^{1}H elastic neutron scattering cross section ratio could provide a new, independent normalization of *np* scattering.

There are many applications that could benefit from better knowledge of the *np* cross section for normalization purposes. Besides its importance for fundamental physics, the interest in high-energy neutron data is rapidly growing because a number of potential large-scale applications involving fast neutrons are under development or have been identified. These applications primarily fall into three sectors: nuclear energy and waste management, nuclear medicine, and radiation effects on electronics.

The recent development of high-intensity proton accelerators has resulted in ideas to use subcritical reactors, fed by neutrons produced in spallation processes maintained by external proton beams, for transmutation of spent fuel from nuclear power reactors or incineration of nuclear weapons

material. This might result in less problematic handling of fissile material. New nuclear data are needed for feasibility assessments of these techniques. The present work is linked to the European Union project HINDAS (high and intermediate energy nuclear data for accelerator-driven systems), which has been organized to meet this demand [13].

Conventional radiation treatment of tumors, i.e., by photons or electrons, is a cornerstone in modern cancer therapy. Some rather common types of tumors, however, cannot be treated successfully using these modalities. For some of these, good treatment results have been obtained with neutron therapy [14].

During the last few years, it has become evident that electronics in aircrafts suffer adverse effects from neutrons generated by cosmic radiation interacting in the upper atmosphere [15,16]. For instance, a neutron could induce a nuclear reaction in the silicon substrate of a memory device, releasing free charge, which could flip one or more memory units. Similar effects causing software or hardware damage have recently been identified at ground level.

Finally, neutrons at commercial aircraft altitudes induce significant radiation doses to the crew [17].

For all the applications mentioned above, an improved understanding of neutron interactions is needed. Neutron cross sections are generally measured relative to the *np* cross section, and therefore the accuracy of most neutron data depend on how well the *np* cross section is known for various angles and energies.

II. EXPERIMENTAL ARRANGEMENT

A. Neutron beam and detector setup

The neutron beam facility (Fig. 1) at the Svedberg Laboratory, Uppsala, Sweden, has recently been described in detail [18], and therefore only a brief outline will be given here. Neutrons of 96 MeV were produced by the ^{7}Li(p,n)^{7}Be reaction when protons hit a neutron production target consisting of lithium enriched to 99.98% in ^{7}Li. The Li target used in the present experiment had a thickness of 427 mg/cm^2 and was bombarded with a proton beam of a few
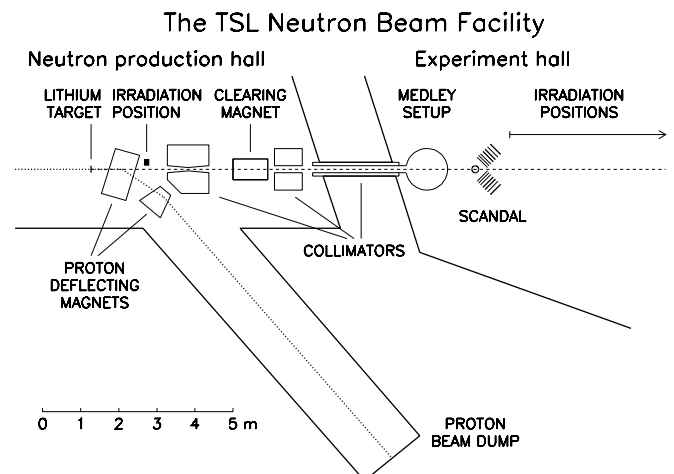

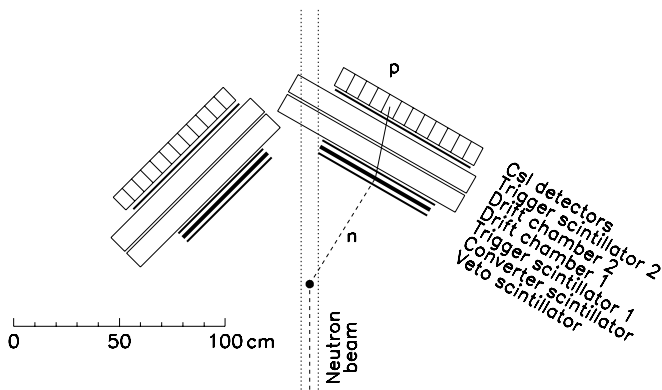FIG. 1. Overview of the TSL neutron beam facility.

FIG. 2. Schematic layout of the SCANDAL setup. In the present experiment, the converter scintillator consisted of two plastic scintillators on each arm. A typical event is indicated.

μA from the Gustaf Werner cyclotron. The resulting neutron spectrum consisted of a peak at 95.6±0.5 MeV with an energy spread of 1.6 MeV full width at half maximum (FWHM) and a low-energy tail which was suppressed by time-of-flight techniques. After the production target, the proton beam was bent into a well-shielded beam dump where the beam current was integrated in a Faraday cup. This procedure left the experimental area essentially background free.

Definition of the neutron beam was accomplished with a system of three collimators. At the scattering target position, the neutron beam was 9 cm in diameter, corresponding to a neutron beam solid angle of 60 μsr, and the yield was typically 4×10^4 s^{-1}cm^{-2}. Finally, the neutron beam was dumped in a tunnel about 10 m downstream of the experimental position.

The neutron beam was transported in a vacuum system which was terminated with a 0.1-mm-thick stainless steel foil, 80 cm upstream of the scattering target position. Immediately after the foil, a fission detector for absolute monitoring of the neutron fluence, based on thin-film breakdown counters (TFBCs) [19], was mounted.

In the present experiment, the SCANDAL (scattered nucleon detection assembly) setup was used (Fig. 2). This detector setup, previously described in Ref. [18], consists of two identical arms positioned on each side of the neutron beam, covering the angular ranges 10°–50° and 30°–70°. In the present experiment, each arm consisted of a 2-mm-thick veto scintillator for charged-particle rejection, two converter scintillators of 20- and 10-mm thickness for neutron-proton conversion, a 2-mm-thick ΔE plastic scintillator for triggering, two drift chambers (DCHs) for proton tracking, another 2-mm-thick ΔE plastic scintillator which was part of the trigger, and an array of CsI detectors (12 on each arm) for energy determination of recoil protons produced in the converter by np scattering. The CsI detectors as well as the plastic scintillators are read out by photomultiplier (PM) tubes. The CsIs have one PM tube each, and the scintillators two each, mounted adjacent to each other on one of the longer, horizontal sides. This design has been chosen to allow the spectrometer arms to be placed close to the beam.

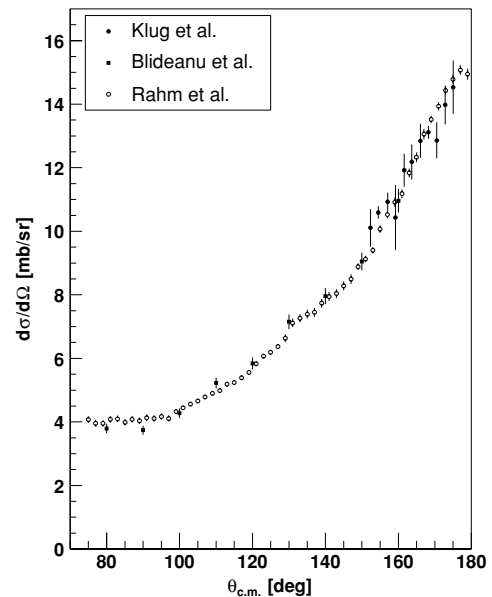The trigger, when detecting neutrons, is defined by a coincidence of the two trigger scintillators, with the most

FIG. 3. Data on np scattering at 96 MeV in the angular range 80°–180° obtained with SCANDAL (Klug *et al.* [18], Blideanu *et al.* [20]). Data on the same reaction at the same energy, obtained with the LISA magnetic spectrometer (Rahm *et al.* [11]), are shown for comparison.

upstream scintillator acting as a veto. The total neutron energy resolution is different for individual CsI crystals, but on average it is 3.7 MeV (FWHM). The variations between the crystals are due to internal properties of the detectors [18].

The SCANDAL setup has been tested using backward np scattering, i.e., by recoil proton detection at 96 MeV [18,20]. Data from these tests are presented in Fig. 3, together with the Rahm *et al.* data obtained with the LISA magnetic spectrometer at the same energy [11]. As can be seen, the most backward data display larger uncertainties than data at more forward angles. This is because SCANDAL was run in a nonstandard configuration very close to the neutron beam, resulting in pileup problems. Additional studies of np scattering by proton detection with SCANDAL as well as another device, MEDLEY [21], are underway [22,23].

B. Experimental procedure

The experiment was carried out during a two-week run with a beam calibration break after the first week of taking data. At the beginning of the campaign, calibration runs were performed by placing a thin CH_2 target in the beam and detecting recoil protons from np scattering. The CH_2 target consisted of several sheets of CH_2 mounted in a multitarget box that allows up to seven targets to be mounted simultaneously, sandwiched between multiwire proportional counters (MWPCs). In this way it was possible to determine in which target the reaction took place, and corrections for energy loss in the subsequent targets could be applied. Two additional MWPCs, located upstream of the targets, acted as veto detectors for charged particles accompanying the neutron

beam. A more detailed description of the multitarget box is given in Ref. [24].

In the multitarget box, two of the target positions were used for graphite targets, allowing a background spectrum of $^{12}C(n,p)$ to be recorded simultaneously. This background was subtracted in order to identify the recoil protons originating from hydrogen in the CH_2 target. The hydrogen peak is, however, already prominent in the CH_2 spectra before subtraction of carbon, since the $^{12}C(n,p)$ reaction has a Q value of -12.6 MeV, which makes the np scattering peak kinematically separated from the carbon background at small angles.

During calibration runs, the trigger condition was changed to include the veto scintillator as well as the two plastic scintillators before and after the DCHs, thus accepting charged particles from the target. After the calibration runs, the trigger was again set for neutron detection, by using the most upstream plastic scintillator as a veto detector for charged-particle rejection. As mentioned earlier, the two detector arms covered the angular regions $10°-50°$ and $30°-70°$. The lower limit of this range, $10°$, represents an arm position where the scintillator detectors barely avoid being hit by the neutron beam and it is the smallest angle where data can be collected with this detector setup. At the largest angle, $70°$, neutrons due to np scattering have too low energy to induce triggers, and therefore no real events are expected in the outermost CsI detectors. The angular region covered by both arms, $30°-50°$, allows studies of the consistency between the two arms.

In the (n,n) measurements, the multitarget box was placed empty upstream of the scattering target and used as an extremely thin charged-particle veto detector. It has, however, been shown that the contamination of charged particles in the neutron beam is very small.

As scattering targets, cylinders of graphite and CH_2 were used, where carbon was treated as a background to $H(n,n)$ events in CH_2. The distribution of beam time between the CH_2 and graphite target was based on an estimation of the number of counts in the carbon background in the region of hydrogen peaks at different angles. The signal-to-background ratio varies dramatically with angle. Since all angles were measured simultaneously, a compromise in the distribution of beam time was necessary. To obtain good statistics in both CH_2 and graphite for all angles, about twice the beam time was spent on CH_2 as on graphite. The two target cylinders had the same size: 16 cm high with a diameter of 8 cm. The graphite cylinder was made of natural carbon with an isotopic composition of 98.9% ^{12}C and had a mass of 1225 g. The CH_2 target consisted of 14.4% H (by mass), and 85.6% C, with a mass of 748.2 g. During the experiment, background data (no target) were also recorded.

Some 80 cm upstream of the scattering target position, the vacuum termination foil and TFBC neutron monitor act as neutron scattering targets. This gives rise to a background of neutrons not originating from the real scattering target, but still triggering the detector setup. SCANDAL is triggered by protons coming from the neutron-proton converter scintillators and cannot distinguish between neutrons coming from the scattering target and neutrons from, e.g., the fission detector. To minimize this source of background neutrons, a lead collimator was installed on both sides of the neutron beam, between

the multitarget box and the scattering target position. The collimator was constructed of 10-cm-thick lead blocks, placed along the neutron beam.

Downstream of the target position, the neutron beam passes through the drift chambers of the arm located at the right-hand side of the beam. The drift chambers contain very little material and are located such that they produce virtually no triggers. Thereby, the setup itself produces very little background. In fact, the background is consistent with elastic neutron scattering in the air surrounding the target.

While the experiment was running, online data were displayed for immediate inspection. Simultaneously, the data were written to tape for subsequent analysis. The dead time in the data acquisition system was around 18, 23, and 3% during CH_2, graphite, and background runs, respectively.

III. DATA ANALYSIS

A. Presorting and calibration

In the offline event-by-event analysis, data were analyzed using the ROOT package from CERN [25]. The first presorting procedure checked that the event was correctly written to tape, and that a number of basic criteria in the CsIs and the drift chambers were fulfilled. It was required that at least one CsI detector in the event had a pulse height (PH) above a certain threshold value. Another requirement was that each event had both vertical and horizontal drift chamber information in two points along the path.

In around 10% of all events, the event contained more than four drift chamber wire hits, mostly due to cross talk between the wires. In those cases, the first firing wire was chosen, since signals induced by cross talk come later in time. This procedure had been investigated earlier using four drift chambers for overdetermination of proton tracks and proved to give the correct result in about 90% of these cases. Hence, it can be estimated that of the order of 1% of all events in a given DCH plane suffer from incorrect trajectory information due to problems with multiple hits in the drift chambers. However, these events can to a large extent be removed by checking the trajectory versus hit in CsI.

Around 60% of all recorded events were rejected during the presorting procedure. The dominating reasons for event rejection was drift chamber inefficiency and too small of an energy deposition in the CsI crystals. As described in Sec. III D, the total drift chamber efficiency, i.e., requiring all four drift chamber planes to give one unique position signal, was around 75%. About 20% of the events were rejected due to energy deposition in the CsI detectors below threshold. Thus, these two effects account for the entire loss in the presorting. In addition, a small fraction (a few percent at most) was rejected due to corrupt information caused by malfunctioning of the data acquisition system. Partly, this seemingly large rejection fraction is due to a relatively relaxed trigger criterion. In this experiment, the count rate is rather low and therefore computer dead time was not a major problem. Therefore, a strategy with generous trigger criteria to minimize the loss of good events was adopted.

Once an event had been accepted in the presorting, it was saved for further analysis. At this point, the conversion point in one of the two converters was calculated. The depth of the conversion [i.e., if the (n, p) reaction occurred in the upstream 20-mm converter or in the downstream 10-mm converter, and at what depth] was determined from pulse height information, and the conversion angle was calculated from DCH trajectory information. At the same time, the elastic neutron scattering angle in the target was calculated from the knowledge of the conversion point, presuming neutron scattering in the target center.

The calibration of the CsIs was made detector by detector with (n, p) data from the calibration runs. In each detector it was possible to identify two calibration points: the pedestal channel and the np proton peak. The pedestal channel was associated with zero energy deposition, and the energy represented by the proton peak was obtained by calculating the energy loss of the proton through the detector setup from the target to the CsI under consideration. The centroid channel was determined by a Gaussian fit to the proton peak.

A linear relationship was assumed between PH and deposited energy. This should be a reasonably good assumption for CsI in the present application [21]. However, detector geometry and local variations in the light output within a CsI crystal caused protons with the same energy to give rise to different PH values along the vertical axis in the crystal. The reason for this vertical dependence is that the crystals have a rather elongated, trapezoidal shape; 30 cm high with a 7×7 cm^2 cross-section area at the PM tube end, and a 5×5 cm^2 area at the other end. If not compensated for, this geometry effect would contribute up to half the intrinsic energy resolution in the CsI detectors. Therefore, when calculating the energy deposited in the CsI crystal, the coordinate of the vertical hit position in the detector was used to select the calibration PH value that correctly corresponded to the np proton peak energy.

After the plastic scintillators were calibrated (described next), the energy deposited by the protons in the CsI detectors was once again checked by subtracting the measured energy losses in the scintillators and the calculated energy losses in other material.

As described earlier, each plastic scintillator has two PM tubes attached to one of the longer horizontal sides. To calibrate them, a region in the center of the scintillator was chosen to obtain a similar distance to both PM tubes. In this case it can be assumed that each PM tube detects half the light from the deposited energy. Also for the scintillators, the pedestal channel and the np proton peak (as defined by the CsI detectors) were used as calibration points. The pedestal channel was taken to represent zero deposited energy, and the energy of the proton peak centroid was obtained from the energy loss calculation in the detectors. A linear correspondence was assumed between PH and deposited energy, and the total deposited energy of a plastic scintillator (ΔE) was obtained by adding the contributions from the two PM tubes.

In the plastic scintillators, geometry effects cause protons with the same energy to give different ΔE signals depending on their location in the detector. This deviation of ΔE from the expected value was mapped over the detectors as a function of

the location in the scintillator, both horizontally and vertically. The effect has been found to be caused to a large extent by the design of the detectors, with both PM tubes situated on the same side. For the 2-mm-thick detectors, the effect is small on an absolute scale, and therefore a compensation was made only for the converter scintillators, with thicknesses of 20 and 10 mm.

To obtain the correct energy loss through the whole detector setup, it was necessary to calculate energy losses in parts of SCANDAL where the protons could not be detected. Such parts are the detector wrappings, drift chamber foils, and air. A calculation of this "undetected" energy loss was based on the detected proton energies in the trigger scintillators and the CsI crystals.

Since there are no excited states in hydrogen, it might seem a bit strange to refer to the hydrogen excitation energy. The SCANDAL setup, however, and all data analysis routines were originally developed for elastic neutron scattering from heavier nuclei, where the excitation energy is a most relevant quantity. The same routines were used when analyzing the present experiment, and therefore the excitation energy was calculated, meaning only that the hydrogen peak appears at zero energy in the analyzed spectra.

In the last step of the calibration process, the total energy of the charged particle was calculated as the sum of all different contributions from the detectors and other material. In regular measurements, the neutron energy at the conversion and the excitation energy were also calculated using the scattering angle, the conversion angle, and the total energy. This gave excitation-energy spectra for 24 different angles in the laboratory system, related to the position of the CsI crystal in which the proton was stopped.

B. Data reduction

Particle identification was achieved by a ΔE-E technique, where the sum of the detected energy losses in the two trigger scintillators was plotted against the energies in the CsI detectors. Particles other than protons (mostly deuterons) arise mainly in the converter scintillators, but they are rarely seen in the CsI detectors, since their energies are in general too low to penetrate the preceding material in the setup.

In the present experiment, each CsI crystal defined an angular bin, and it was considered important to associate every elastically scattered event with one specific CsI. Furthermore, energy determination for protons that passed through more than one CsI crystal was very poor due to large straggling effects in CsI wrapping material. Consequently, a position gate was applied on every crystal, ensuring that an accepted proton was stopped in a single CsI detector.

Events from the low-energy tail of the neutron spectrum were rejected using a cut on the neutron time of flight (TOF). The TOF was defined as the time difference between the first trigger detector and a signal from the cyclotron radio-frequency (RF) system. There is, however, no background from low-energy neutrons in the energy region of the elastic peak. The reason is that a low-energy neutron, i.e., from wrap-around effects, cannot induce emission of a full-energy
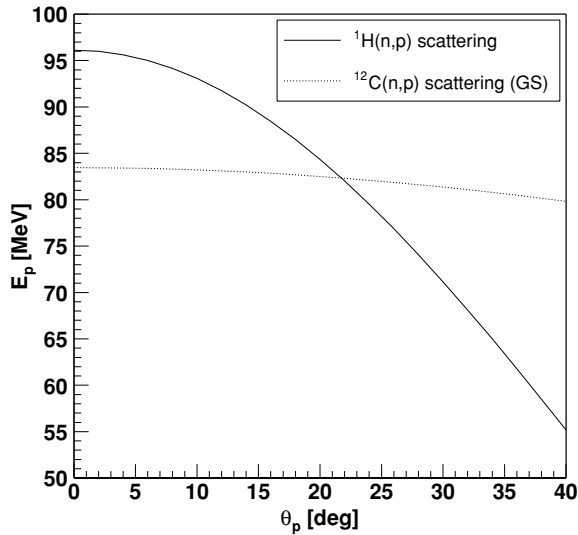
FIG. 4. Laboratory system kinematics of proton emission from hydrogen and the carbon ground state. At small angles, the proton emission is kinematically well separated, while at about 20°, the two reactions coincide. An opening angle criterion of 10° was used in the analysis.

neutron from the scattering target. The TOF cut was therefore not important in this experiment.

The conversion of neutrons to protons in the converter scintillators can occur through the $^{12}C(n, p)$ reaction, besides the H(n, p) reaction, since the scintillators contain carbon as well as hydrogen. On the other hand, the Q value for $^{12}C(n, p)$ is -12.6 MeV, meaning that at forward angles, an energy cut is sufficient to separate the two reactions (see Fig. 4). However, at a conversion angle of about 20°, the proton energies from the two processes overlap, and it cannot be determined whether np scattering or the $^{12}C(n, p)$ reaction is responsible for the conversion. To resolve this ambiguity, a maximum conversion angle criterion was applied, demanding that the conversion angle be less than 10°.

About two thirds of the events were found to have converted in the thicker upstream detector, as was expected. Later in the analysis, however, it proved difficult to use the events from the thick converter because its energy resolution was poor (4 MeV compared to 2 MeV for the thinner converter); and since statistics were sufficiently good using only the thinner converter, the events from the thick one were discarded.

C. Extraction of elastic scattering events

So far the analysis had been done on an event-by-event basis, and when all cuts had been applied the result was excitation-energy spectra at 24 angles (corresponding to the 24 CsI detectors) in the range 10°–70° in the laboratory system. It was, however, not possible to extract peaks for the largest angles, so in reality spectra were obtained for 12 angles between 10° and 38° in the laboratory system. Since the measurement was made with two detector arms, partly overlapping each other in angular range, two sets of data were obtained, one ranging from 10° to 38° and the other from 26° to 38°.

All cuts were applied in the same way for CH$_2$, graphite, and background (no target) runs. For all runs, the hydrogen mass was used in kinematics calculations when defining the excitation energy.

For the further analysis, the energy spectra were stored as histograms. Examples are shown in Fig. 5. By subtracting background and carbon from CH$_2$, hydrogen spectra were obtained. In a first step, background spectra were subtracted from both graphite and CH$_2$ for each CsI. Background and signal spectra were normalized to the same neutron fluence (given by the fission monitor) and corrected for dead time. In the second step, the carbon content was subtracted from CH$_2$, taking into account the contents of carbon nuclei in the two samples.

A fact to consider when subtracting carbon from CH$_2$ is the difference in attenuation in the two target samples. The targets have the same dimensions, but different densities and chemical compositions. In the graphite target, the attenuation is due to nuclear reactions in carbon. In the CH$_2$ target, on the other hand, both the hydrogen and carbon nuclei are important, and all hydrogen interactions are considered as attenuation, since a neutron scattered from hydrogen essentially always loses enough energy to be regarded as lost from the flux of the incoming neutrons. Attenuation correction coefficients, calculated from the carbon reaction cross section and the hydrogen total cross section, were applied to the spectra before subtraction. These coefficients were estimated from an assumption of the mean path traveled in the sample by the neutrons before and after scattering, based on a Monte Carlo simulation [26]. Since the attenuation is energy dependent, different correction coefficients were applied for different CsI detectors.

Because of the relatively large scattering targets used in this experiment, it was necessary to investigate the effects of multiple scattering caused by carbon in the targets. The graphite and CH$_2$ targets were of the same size, but their carbon contents were quite different, resulting in a larger fraction of multiple-scattered events from the graphite sample. To investigate the effect, a Monte Carlo code [26] was used to simulate the multiple scattering of neutrons from carbon in the two scattering targets. This gave an estimate of how much the cross section changed for every angular bin because of multiple scattering, and spectra were multiplied by these coefficients before the carbon subtraction. The effect was found to be of importance only at the two most forward CsI detectors (at angles 10° and 14° in the laboratory system). At 10° the correction for multiple scattering was around 5% in CH$_2$ and 7% in graphite.

In parallel with signal histograms, variance histograms were obtained by performing the corresponding operations. These histograms were used for calculation of the statistical uncertainties.

D. Cross-section determination and normalization

When determining the angular distribution of the elastic neutron scattering cross section, the number of scattering events in every CsI was obtained from the hydrogen
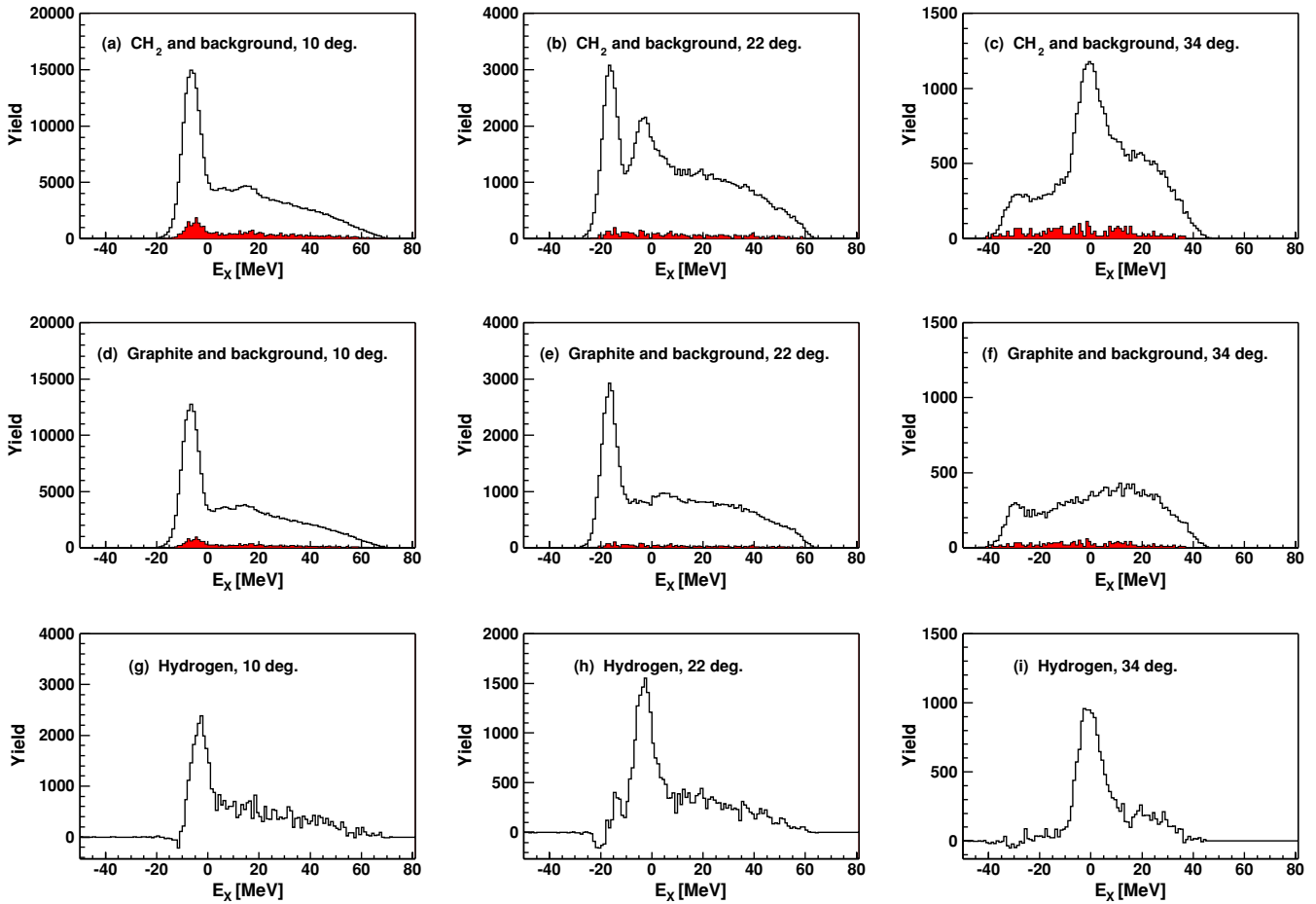
FIG. 5. (Color online) Energy spectra for CH_2, graphite, and hydrogen shown at three different angles in the laboratory system: $10°$, $22°$, and $34°$. In the upper panels, CH_2 spectra are presented together with background (no target) spectra. In the middle panels, graphite and background spectra are shown, and in the lower panels the hydrogen spectra. The tails in the hydrogen spectra are caused by the low-energy neutron beam continuum.

histograms, the number of neutrons in the beam was given by either the fission counter or the integrated proton beam current, and the number of target nuclei was calculated from the density, volume, and chemical composition of the scattering target.

The solid angle for protons detected in the CsI crystals is different from detector to detector, depending on different distances to the scattering target and individual sizes of the accepted regions (position hit gates) of each crystal. Also, the neutron energy (which varies with neutron angle) is important because it affects the conversion probability in the converter as the np cross section is energy dependent. These effects give rise to an individual effective solid angle for every CsI detector, which is due to both the geometric solid angle for that CsI crystal and the probability that a conversion proton hits the crystal. To calculate these solid angles, a computer code recently described in [12] was used. The same code was used to calculate the average elastic neutron scattering angle associated with each CsI detector, and the angular range covered.

The proton detection efficiency has components from the drift chamber efficiency, the efficiency of selecting the correct

DCH wire in multiple-hit events, and the CsI response. The drift chambers consist of four detection planes on each arm, with a combined efficiency that has previously been measured to 0.75 ± 0.10 (from an average of 0.93 per plane). The efficiency of selecting the correct wire has been measured to 0.93 (from 0.98 per plane). No energy dependence in the DCH efficiencies has been found for a given set of detector parameters. The CsI response varies with energy and gives different detection efficiencies for crystals at different angles. This occurs because some protons undergo nuclear reactions before coming to rest in the CsI, resulting in the loss of light [18].

The low-energy continuum originating from the ^{7}Li(p,n) reaction contributes to the full-energy np peaks, and hence to the ground state peaks in the excitation-energy spectra. This effect is different for different CsIs because of the variations in energy resolution. The contribution from the low-energy neutrons is a function of the peak width [27] and has been determined using experimental neutron spectra for the ^{7}Li(p,n) reaction measured by Byrd and Sailor [28]. These correction factors were then used in the cross section

calculations. For some CsIs, the effect was quite large (up to 20%), while a more normal value of the correction was between 6 and 11%.

The number of elastic scattering events at each angle was obtained by integrating the corresponding peaks in a region of $\pm\Gamma$ around the peak centroid, where Γ is the full width at half maximum (FWHM). The centroid of the peak and the width Γ were obtained from a Gaussian fit to the peak.

When all corrections had been taken into account, the final angular distribution for the forward np scattering cross section was obtained. The absolute scale was given by the TFBC neutron monitor which in itself has an uncertainty of more than 10%, making further normalization necessary.

The data were normalized to the total np cross section in the following way. As described in Sec. III C, the present data consist of two subsets from the two SCANDAL detector arms, i.e., SCANDAL left and SCANDAL right. These two sets were to be combined with the earlier data by Rahm *et al.* using the LISA magnetic spectrometer [11] to form one data set covering the angular interval 20°–180° in the center of mass (c.m.) system. To obtain a single relative distribution, the three subsets were internally normalized using the Nijmegen partial wave analysis PWA93 [29]. The two SCANDAL data sets were normalized to PWA93 in the angular region where the arms overlap, i.e., in the range 50°–76°, and the LISA data were normalized to PWA93 in the equally large angular range 75°–101°. The factors used in this procedure were 1.02, 1.08, and 1.03 for SCANDAL left, SCANDAL right, and LISA, respectively. A final normalization of the combined data set to the total np cross section measured with high precision by Lisowski *et al.* [30] was then made, using Eq. (1). The normalization factor needed this time was 0.978.

Note that the SCANDAL arms needed renormalization of 0% (1.02 × 0.978) and 6%, which is satisfactory considering that the uncertainty in the neutron monitoring alone is around 10% [18]. The renormalization of the Rahm data is 0.7%, which is well within the normalization uncertainty of 1.9% stated in [11].

The original Rahm data were normalized in a procedure where the fraction of the total cross section due to np scattering in the studied angular range (74°–180°) was deduced from a set of partial wave analyses and potential models [11]. This fraction was estimated to be 61.3±1.5%. In the present work, such a procedure is no longer necessary, but the resulting data set can be used to inspect this previously estimated fraction. In the present data set, 61.8±0.5% of the total cross section is accounted for by the differential np cross section in the 74°–180° range, i.e., the result is in good agreement with the previous estimate.

Other methods of normalization were also attempted. From the CH$_2$ spectra, it was possible to analyze elastic neutron scattering from carbon and compare it to elastic neutron scattering from hydrogen at the same laboratory angle. For five CsIs where the peaks were prominent and resolved, the ratios between the number of counts in the carbon and hydrogen peaks were extracted and related to the expected ratios in cross sections. From knowledge of the carbon cross section for a specific angle, the expected hydrogen cross section was calculated and compared to the actual measured cross section

for that CsI. As a carbon reference cross section, the fit to the ^{12}C(n,n) data in Fig. 5 of Klug *et al.* [12] was used. The fit to the data was made using a parametrization by Koning and Delaroche [31]. The ratio between the reference hydrogen cross section and the measured one was on average 0.94±0.03±0.11, where the first uncertainty is the statistical error, and the second is the systematic error of the method. The latter was estimated from the standard deviation of the spread in results between the five CsIs.

Thus, on average this normalization technique deviates from normalization to the total cross section by 6%, with a 3% statistical error. The ^{12}C(n,n) reference cross section has been estimated to have a 3% uncertainty [12]. Thus, the average deviation is in reasonable agreement with what can be expected from those uncertainties only. The systematic uncertainty (11%) is, however, significantly larger than the statistical error; therefore it seems more correct to assign an uncertainty to this method of at least 10%. The reason for the larger systematic uncertainty is at least partly due to the different behavior of the angular distributions of elastic neutron scattering from ^{12}C and ^{1}H. The former has a very steep angular distribution, where the cross section changes by about 20% per degree, while the np scattering cross section changes much less (typically 2% per degree). Hence, the obtained systematic uncertainty of 11% corresponds to an uncertainty in the absolute angle of around 0.5°, i.e., less than the angular uncertainty of the present experiment.

The method above relies on only a few data points. Still, the possibility that a better normalization might result from a larger set of data should be investigated. Therefore, the full angular distribution of ^{12}C(n,n) was extracted from the graphite target data. This angular distribution was then used to derive a value of the total elastic cross section, resulting in a value 18% lower than the experimental value derived from the difference of the total and the reaction cross sections.

It might seem surprising that relative normalization of ^{12}C versus ^{208}Pb can be performed with a 3% uncertainty while normalization of ^{12}C versus ^{1}H results in discrepancies of 10% or more. The properties of these normalization techniques can be understood from the information displayed in Fig. 6. In the upper panel, the differential cross sections for neutron scattering from ^{1}H, ^{12}C, and ^{208}Pb are shown in parametrized form. As can be seen, the cross sections for ^{12}C and ^{208}Pb have a similar overall slope, but the ^{208}Pb data display more structure. Compared with scattering from these nuclei, the np scattering angular distribution is much flatter.

As can be seen in Fig. 6, the Pb/C ratio fluctuates significantly, but if integrated over a wide angular range, these oscillations more or less cancel. Thus, normalizing in a single point could produce results that are significantly off, but using the entire angular distribution for normalization, as in Ref. [12], would likely compensate for a small mismatch in angle. The C/H ratio is more difficult to use for normalization because there is no "built-in" compensation. Over the entire 10°–60° range, a 1° error in absolute angle results in a cross section ratio 10–15% different from the expected, and integration over a wider angular range does not remedy the problem. Thus, to employ the C(n,n) cross section as reference for normalization of np scattering to a precision of 2%, i.e., similar to what can
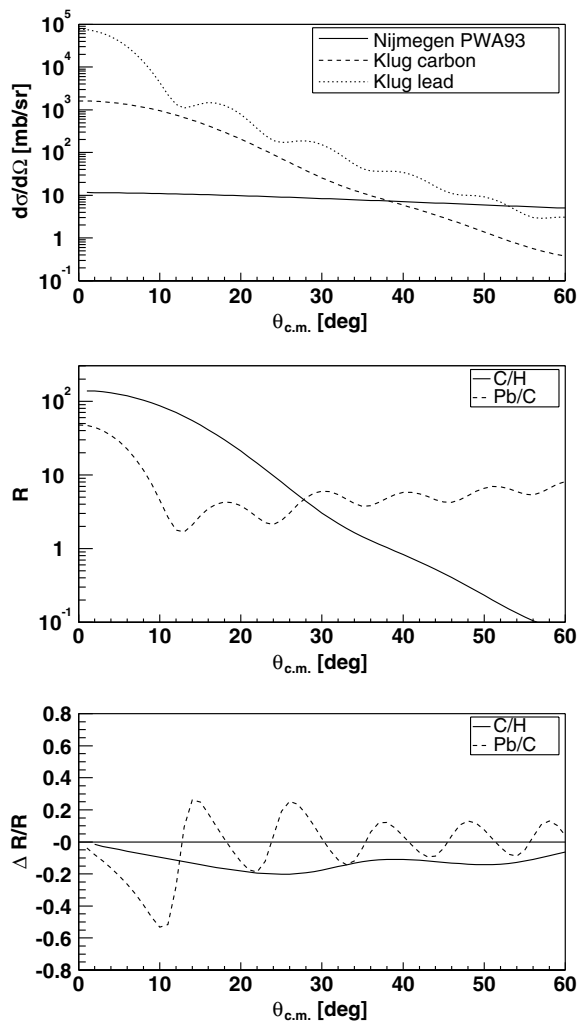
FIG. 6. In the upper panel, predictions of angular distributions of elastic neutron scattering from hydrogen, carbon, and lead at 96 MeV are shown. The lead (dotted line) and carbon (dashed line) data are fits to the data of Klug *et al.* [12] using the optical model parametrization by Koning and Delaroche [31]; the solid line is the Nijmegen partial wave analysis PWA93 [29]. In the middle panel, the ratio between the carbon and hydrogen cross sections is shown together with the ratio between the lead and carbon cross sections. In the lower panel, the relative changes in these ratios per degree scattering angle are shown. See the text for further details.

be obtained with normalization to the total np cross section, an absolute angular uncertainty of less than $0.2°$ is required. With the experimental techniques of today, this would require smaller targets and larger distances to the detector, which would demand very long experimental runs.

E. Estimation of experimental uncertainties

In the present experiment, the relative differential cross section was measured and then normalized using independent information. Uncertainties that affect all angles equally (e.g., drift chamber inefficiencies, neutron monitoring, and computer dead time) are therefore taken care of by the normalization procedure. Other uncertainties, however, are angle dependent and must somehow be quantified, since they can affect the

shape of the angular distribution. Some of these effects can easily be modeled and corrected for, such as the different energy losses through the SCANDAL setup caused by its geometry.

Among the corrections that vary with angle is the contribution to the np scattering peak from the low-energy continuum of the $^7Li(p,n)$ spectrum. This contribution gives an uncertainty in the peak content, which varies with peak width. Assuming the uncertainty to be 10% of the correction, this effect induces an error in cross section of up to 2% in the worst case. For most angles, however, the uncertainty is around 1% or smaller.

Another uncertainty comes from the procedure of determining integration limits by fitting Gaussians to the elastic scattering peaks. Varying the Gaussian fits and thereby the integration intervals within the uncertainties revealed that the total resulting uncertainty in the cross section was around 2% for all angles.

The subtraction of carbon from CH_2 induces an angle-dependent uncertainty which has several contributions. First of all, the random error due to counting statistics affects each CsI differently since the signal-to-background ratio depends strongly on angle. At small angles, where the carbon and hydrogen peak overlap in energy, the statistical error in hydrogen is as large as 3.5%.

Another effect correlated to the subtraction is the correction for attenuation in the targets. To make the subtraction coefficients correct, the attenuation correction has to be done first. Its uncertainty has a large impact on the resulting hydrogen spectra at forward angles, where the cross section results from the subtraction of two large numbers. The uncertainty in attenuation was assumed to be at most 10% of the correction, coming from uncertainties in the involved cross sections and calculation of the mean path traveled by neutrons in the targets. The attenuation in graphite and CH_2 are correlated, however, since the carbon reaction cross section enters in both cases, as well as the calculation of the mean path. With this taken into account, the uncertainty in the resulting experimental np cross section was estimated to be around 0.5% except at the smallest angles where the effect was significantly larger (up to 6%).

Finally, the subtraction uncertainty depends on the uncertainty in the correction for multiple scattering, which was again taken to be 10% of the correction itself. This correction was made for the two smallest angles only, but since the corrections for graphite and CH_2 were treated as uncorrelated, it had a large impact on the resulting np cross section. For the smallest angle, the uncertainty in the final result due to the uncertainty in the multiple scattering correction was 10%.

The solid-angle calculation depends on several factors, such as the size of the target and the accepted area on the CsI detectors. The latter depends on the position uncertainty in the drift chambers, resulting in an area uncertainty of typically 3.2% [18]. This uncertainty affects individual CsI detectors differently.

The average angle seen by each CsI detector is the mean of a distribution with r.m.s. values around $1.9°$. To be able to extract the angular distribution of the cross section, it is important to know the angles at which the detectors were situated. The inherent angular uncertainty has been estimated

to be about 0.5°, having components from the uncertainty in the positions of the target, the drift chambers, and the detector arms. These effects result in an equal shift of all detector angles on the same detector arm. In addition, each drift chamber contains many drift cells that act as independent detectors with an uncertainty in position information of around 0.5 mm, resulting in a negligible uncertainty in the present experiment. Presuming that the centroid of a distribution can be determined with an accuracy of 0.5 σ, the uncertainty in angle due to the extension of the target is close to 1.0°. With the inherent angular uncertainty of the setup added in quadrature, the resulting total angular uncertainty is estimated to be 1.1°.

In the present measurement of forward *np* scattering, different normalization factors were needed for the data points from the two detector arms, i.e., SCANDAL left and SCANDAL right. The normalization factor for SCANDAL left was 1.00, and the factor for SCANDAL right was 1.06. The fact that two detection systems were used allows some further investigation of the systematic uncertainties in the present experiment. In the normalization procedure, the absolute scale of the two SCANDAL arms differed by 6%. In this comparison, all uncertainties related to drift chamber inefficiencies come into play. This means that a 1% uncertainty in the efficiency per plane can easily account for the entire difference.

A second test is provided by four pairs of data points, measured at about the same angle but with different SCANDAL arms. After normalization of both arms, internal differences in these pairs beyond statistical errors (which are small) should reflect the systematic uncertainties involved. The average pairwise difference is 7.7%, while the expected difference from the estimated systematic uncertainties is 5.9%. Thus, the difference is in reasonable agreement with expectations.

IV. RESULTS AND DISCUSSION

The results of the present work consist of two parts: first, the forward-angle *np* data measured in the present experiment and presented in Table I, and second, the backward-angle *np*

data previously reported in [11] and now renormalized and presented in Table II. For the forward-angle data, the table gives the statistical as well as the systematic errors separately; while for the backward-angle data, total errors are given as the quadratic sums of the statistical and systematic uncertainties. Errors due to normalization are not included. Neither are other uncertainties that equally affect the data points since they vanish with the adopted normalization method.

Together, these two data sets cover an angular range of 160° in the c.m. system, i.e., the angles 20°–180°. The results are shown in Fig. 7, where the upper panel presents the angular distribution of the two data sets together with Nijmegen PWA93 [29], and the lower panel shows the same information multiplied by the solid-angle element to illustrate the importance of each data point in the normalization to the total hydrogen cross section.

The upper panel of Fig. 8 shows data from the present experiment together with other forward *np* scattering data at 90–100 MeV from the literature, i.e., data from Chih *et al.* [32], Griffith *et al.* [33], Bersbach *et al.* [34], and Scanlon *et al.* [35]. The same panel shows the partial wave analyses Nijmegen PWA93 [29] and SAID SP03 [36]. The lower panel of Fig. 8 compares data with three potential models, the Nijm93 [37], CD Bonn [38,39], and Paris [40] potentials. In this panel, data are plotted with both statistical and total errors.

A simple check of the data is provided by Wick's limit [41,42]. One can derive from very fundamental quantum mechanics relations [43] that the differential cross section at 0° must exceed a value related to the total cross section,

$$\frac{d\sigma(0°)}{d\Omega} \geqslant \left(\frac{\sigma_T}{4\pi\bar{\lambda}}\right)^2. \qquad (2)$$

Since the total cross section is very well known, this can provide a very stringent test of the data. For *np* scattering at 96 MeV, Wick's limit is 9.09±0.09 mb/sr. As can be seen from Table I and in Figs. 7 and 8, the differential cross section clearly exceeds this value and thus obeys the relation.

In Table III, χ^2/N values for the forward *np* data compared with the different PWAs and potentials are presented. χ^2/N

TABLE I. Differential cross sections for forward *np* scattering at 96 MeV. The first error is the statistical error; the second is the estimated systematic error excluding normalization uncertainty.

$\theta_{c.m.}$ (deg)	$d\sigma/d\Omega$ (mb/sr)	$\Delta d\sigma/d\Omega$ statistical (mb/sr)	Δrel. (%)	$\Delta d\sigma/d\Omega$ systematic (mb/sr)	Δrel. (%)	SCANDAL arm (L or R)
19.9	10.68	0.37	3.5	1.31	12.3	R
27.0	9.82	0.32	3.3	0.65	6.6	R
34.2	7.39	0.17	2.3	0.31	4.2	R
42.5	7.63	0.13	1.7	0.30	3.9	R
50.0	5.70	0.11	1.9	0.23	4.0	R
51.6	6.31	0.16	2.5	0.25	4.0	L
58.2	5.08	0.09	1.8	0.21	4.1	R
58.9	4.54	0.12	2.6	0.18	4.0	L
66.5	4.33	0.11	2.5	0.18	4.2	L
66.9	4.48	0.08	1.8	0.18	4.0	R
74.6	4.28	0.10	2.3	0.18	4.2	L
75.6	4.03	0.07	1.7	0.18	4.5	R

TABLE II. Renormalized differential cross sections for backward *np* scattering at 96 MeV. Original data are from Rahm *et al.* [11].

$\theta_{c.m.}$ (deg)	$d\sigma/d\Omega$ (mb/sr)	$\Delta d\sigma/d\Omega$ (mb/sr)	Δrel. (%)	$\theta_{c.m.}$ (deg)	$d\sigma/d\Omega$ (mb/sr)	$\Delta d\sigma/d\Omega$ (mb/sr)	Δrel. (%)
75	4.10	0.11	2.7	129	6.68	0.12	1.8
77	3.99	0.11	2.8	131	7.17	0.13	1.8
79	3.99	0.11	2.8	133	7.31	0.13	1.8
81	4.11	0.11	2.7	135	7.44	0.14	1.9
83	4.13	0.11	2.7	137	7.51	0.14	1.9
85	4.02	0.10	2.5	139	7.70	0.14	1.8
87	4.11	0.10	2.4	141	8.01	0.14	1.7
89	4.07	0.10	2.5	143	8.10	0.14	1.7
91	4.16	0.10	2.4	145	8.34	0.14	1.7
93	4.14	0.10	2.4	147	8.55	0.15	1.8
95	4.20	0.10	2.4	149	8.95	0.10	1.1
97	4.14	0.10	2.4	151	9.19	0.10	1.1
99	4.36	0.06	1.4	153	9.47	0.10	1.1
101	4.47	0.06	1.3	155	10.14	0.12	1.2
103	4.59	0.06	1.3	157	10.60	0.12	1.1
105	4.69	0.06	1.3	159	11.00	0.14	1.3
107	4.82	0.06	1.2	161	11.26	0.14	1.2
109	4.93	0.06	1.2	163	11.92	0.14	1.2
111	5.02	0.07	1.4	165	12.42	0.15	1.2
113	5.22	0.07	1.3	167	13.15	0.16	1.2
115	5.28	0.07	1.3	169	13.62	0.12	0.9
117	5.43	0.06	1.1	171	14.04	0.13	0.9
119	5.60	0.06	1.1	173	14.53	0.13	0.9
121	5.88	0.07	1.2	175	14.89	0.14	0.9
123	6.12	0.07	1.1	177	15.19	0.15	1.0
125	6.24	0.07	1.1	179	15.05	0.17	1.1
127	6.41	0.07	1.1				

was calculated both with only statistical errors in the data and with statistical as well as systematic errors. Generally, using only the statistical uncertainties result in a high χ^2/N (around 9), while including the systematic uncertainties pushes the χ^2/N down to around 2. These results seem to corroborate our previous conclusion that the statistical errors are not dominating. Instead, the systematic uncertainties are in general more important. When including these, the χ^2/N values are dramatically reduced, down to reasonable values.

It is interesting to note that the data do not seem to favor any particular potential model or partial wave analysis; they all result in very similar χ^2/N values. As can be seen in Fig. 8, a significantly improved data quality would be needed to distinguish between these theory models. It is notable that no experiment in the 90–100 MeV range is even near the precision required to favor one model over another in the forward angular range. Since the limiting factors in the present experiment are systematic effects that cannot be significantly improved upon, it can be concluded that a fundamentally different experimental approach is needed to reach such a precision.

A novel approach in experimental studies of *np* scattering has recently been attempted at the Indiana University Cyclotron Facility (IUCF) [44]. Neutrons are produced by the ^{2}H$(p,n)^2$He reaction, where ^{2}He denotes two correlated protons. Thus, by coincident detection of two low-energy protons,

a beam of "tagged" neutrons can be produced, as discussed in Sec. I. This beam has a low but well-known intensity and can be used to measure the *np* scattering cross section. The aim has been to reach an uncertainty of a few percent, i.e., resembling the quality of experiments using the total *np* cross section for normalization. Results of a measurement at 194 MeV have been presented recently [45] and further data analysis is in progress. The technique as such could in principle be used also at the energy of the present work.

Assessment of the resulting total uncertainty in the overall normalization is not straightforward. With the adopted method, there is an uncertainty contribution from the uncertainty in the total cross section, which is estimated to be 1.0% at the present energy, based on an investigation of the data by Lisowski *et al.* [30]. In addition, there is a contribution due to the uncertainty in absolute energy in the present experiment, because the total cross section changes with energy. The latter contribution is estimated to be 0.6% based on an analysis of the total cross section slope in the present region. These two effects added in quadrature results in a 1.1% normalization uncertainty [11].

If the shape of the differential cross section were perfectly measured, there would be essentially no additional uncertainties involved, since the statistical uncertainty in the data would be negligible. However, any distortions in the shape of the angular distribution could lead to a normalization
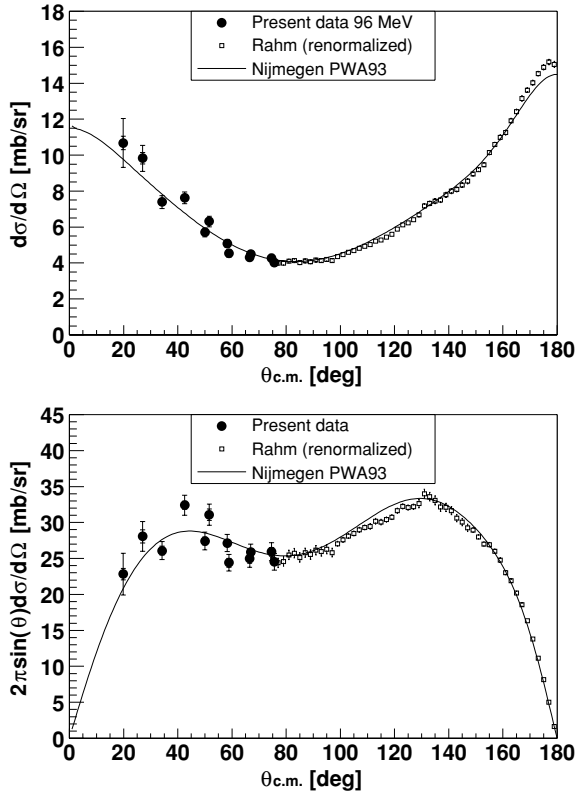
FIG. 7. Angular distributions of *np* scattering cross sections at 96 MeV. Filled circles represent the present data and open squares are the renormalized Rahm *et al.* data [11], i.e., the data of Table II. In the upper panel, experimental differential cross sections are shown together with the Nijmegen partial wave analysis PWA93 [29]. In the lower panel, data and PWA93 have been multiplied with the solid-angle element $2\pi \sin \theta$ to illustrate the relative weight in the normalization to the total cross section. In both panels, the present data are shown with double error bars; the inner bars representing the statistical error, and the outer the statistical and systematic errors, excluding normalization errors, added in quadrature.
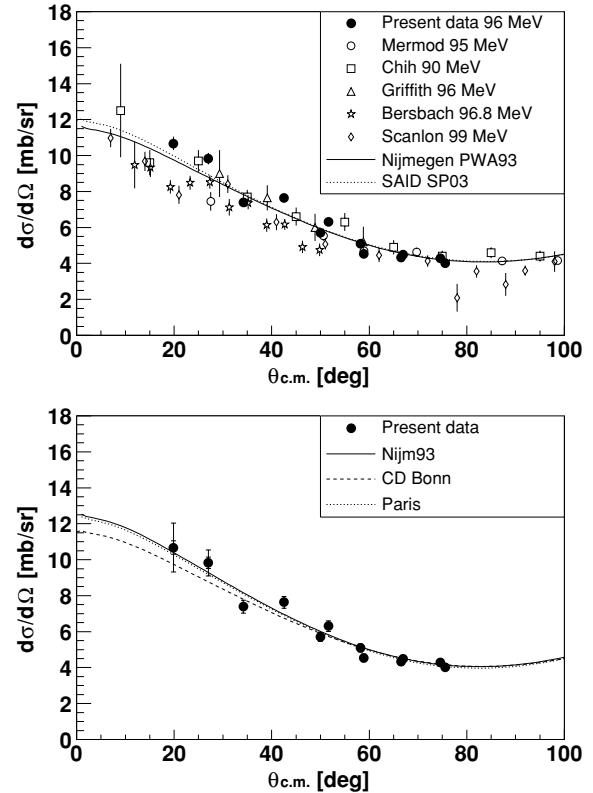
FIG. 8. Differential scattering cross sections of the present work (filled circles). In the upper panel, data are shown together with the Nijmegen PWA93 [29] and SAID SP03 [36] partial wave analyses and with experimental data in the energy region 90–100 MeV from the literature [22,32–35]. In the lower panel, the present data are compared with the Nijm93 [37], CD Bonn [38,39], and Paris [40] potentials. The lower panel gives both the statistical errors (the inner error bars) and the statistical and the systematic errors, excluding normalization errors, added in quadrature (the outer error bars).

error. This possibility has been investigated as described below.

The Rahm *et al.* data at backward angles were obtained by a technique where data from a number of overlapping angular regions were added to a joint data set. This allowed an estimation of the uncertainty in the 90°/180° cross-section ratio, based on the statistical errors in the overlap regions, which was found to be 2.2%. In the present work at forward angles, the 20°/75° ratio has a 3.9% statistical uncertainty. The systematic uncertainty is larger, but to some extent correlated. If we use the full experimental data set, ranging from 20° to 180°, but distort the shape of it and subsequently normalize it with the prescription described in this paper, we arrive at slightly different values of the differential cross section. We used a distortion that increases the 0° and 180° differential cross sections before normalization with 2%, while keeping the 90° differential cross section unchanged, and all other cross sections modified with a linear function, i.e., a distortion function looking like the letter V. With such a distortion, the differential cross sections change by up to 1.5% at the worst

angle, which is at 20°, i.e., the small-angle limit of the present data set. The change at 180°, i.e., where the cross section has the largest impact in determinations of the pion-nucleon coupling constant, is 1.1%.

It should be pointed out that the *np* data presented are not the only important results, but also the findings from investigations of measurement techniques and normalization methods. The

TABLE III. χ^2 per degree of freedom for the present data compared to various PWAs and NN potentials. Results are shown for when the statistical error only is considered and for when both the statistical and systematic uncertainties, excluding normalization errors, are taken into account.

Potential or PWA	χ^2/N Statistical error	χ^2/N Total error
PWA93	9.48	1.98
SP03	9.73	2.07
Nijm93	8.04	1.80
CD Bonn	9.34	1.94
Paris	7.67	1.70

present experiment reached a very high level of accuracy, given that it dealt with neutrons both in the incident and exit channel. Two independent detector systems of equal design agree absolutely on the overall scale to within 6%, and the spread in individual data points using either one or the other is about 8%. Moreover, the two detection systems do not only agree internally to a few percent, but also absolutely. After analysis and corrections, the two arms needed renormalization of 0 and 6%, which are remarkably small numbers for this type of experiment.

With the present data in the $20°$–$75°$ range, the normalization of the previous data by Rahm *et al.* [11] in the $74°$–$180°$ range could be cross-checked. This resulted in a renormalization of these data of 0.7%, i.e., within the reported uncertainty of 1.9%.

A novel technique for absolute scale normalization has been tested and found to have about 10% uncertainty for the present purpose, i.e., normalization of np scattering data using $^{12}C(n,n)$ data as reference. With the present uncertainties of about 10% in the np scattering database, a normalization method should have uncertainties significantly smaller than that to provide useful guidance. Thus, it can be concluded that the new method is not very decisive in the quest for the np scattering cross section.

[1] J. Blomgren, N. Olsson, and J. Rahm, Phys. Scr. **T87**, 33 (2000).

[2] B. E. Bonner, J. E. Simmons, C. L. Hollas, C. R. Newsom, P. J. Riley, G. Glass, and Mahavir Jain, Phys. Rev. Lett. **41**, 1200 (1978).

[3] M. L. Evans *et al.*, Phys. Rev. Lett. **36**, 497 (1976).

[4] M. L. Evans *et al.*, Phys. Rev. C **26**, 2525 (1982).

[5] Mahavir Jain *et al.*, Phys. Rev. C **30**, 566 (1984).

[6] L. C. Northcliffe, Mahavir Jain, M. L. Evans, G. Glass, J. C. Hiebert, R. A. Kenefick, B. E. Bonner, J. E. Simmons, C. W. Bjork, and P. J. Riley, Phys. Rev. C **47**, 36 (1993).

[7] W. Hürster, Th. Fischer, G. Hammel, K. Kern, M. Kleinschmidt, L. Lehmann, H. Schmitt, L. Schmitt, and D. M. Sheppard, Phys. Lett. **B90**, 367 (1980).

[8] J. Franz, E. Rössle, H. Schmitt, and L. Schmitt, Phys. Scr. **T87**, 14 (2000).

[9] B. E. Bonner (private communication).

[10] J. Blomgren, in *Proceedings of Workshop on Nuclear Data for Science & Technology: Accelerator Driven Waste Incineration*, Trieste, Italy, Sept. 10-21, 2001, edited by M. Herman, N. Paver, and A. Stanculescu, ICTP Lecture Notes **12**, 327 (2002).

[11] J. Rahm *et al.*, Phys. Rev. C **63**, 044001 (2001).

[12] J. Klug *et al.*, Phys. Rev. C **68**, 064605 (2003).

[13] A. Koning *et al.*, J. Nucl. Sci. Tech. Suppl. **2**, 1161 (2002).

[14] A. Wambersie, P. Pihet, and H. G. Menzel, Radiat. Prot. Dosim. **31**, 421 (1990).

[15] H. H. K. Tang, IBM J. Res. Develop. **40**, 91 (1996).

[16] J. Blomgren, B. Granbom, T. Granlund, and N. Olsson, Mat. Res. Soc. Bull. **28**, 121 (2003).

[17] D. T. Bartlett, R. Grillmaier, W. Heinrich, L. Lindborg, D. O'Sullivan, H. Schraube, M. Silari, and L. Tommasino, Radiat. Res. Cong. Proc. **2**, 719 (2000); see also the entire issue of Radiat. Prot. Dosim. **86(4)** (1999).

[18] J. Klug *et al.*, Nucl. Instr. Meth. Phys. Res. A **489**, 282 (2002).

[19] A. N. Smirnov, V. P. Eismont, and A. V. Prokofiev, Rad. Meas. **25**, 151 (1995).

[20] V. Blideanu *et al.*, Phys. Rev. C **70**, 014607 (2004).

[21] S. Dangtip *et al.*, Nucl. Instr. Meth. Phys. Res. **A452**, 484 (2000).

[22] P. Mermod *et al.*, Phys. Lett. **B597**, 243 (2004).

[23] P. Mermod *et al.* (unpublished).

[24] H. Condé *et al.*, Nucl. Instr. Meth. Phys. Res. A **292**, 121 (1990).

[25] R. Brun and F. Rademakers, Nucl. Instr. Meth. Phys. Res. A **389**, 81 (1997); see also http://root.cern.ch/.

[26] B. Holmqvist, B. Gustavsson, and T. Wiedling, Ark. Fys. **34**, 481 (1967); modified version by N. Olsson (unpublished).

[27] J. Rahm *et al.*, Phys. Rev. C **57**, 1077 (1998).

[28] R. C. Byrd and W. C. Sailor, Nucl. Instr. Meth. Phys. Res. A **264**, 494 (1989).

[29] V. G. J. Stoks, R. A. M. Klomp, M. C. M. Rentmeester, and J. J. de Swart, Phys. Rev. C **48**, 792 (1993).

[30] P. W. Lisowski, R. E. Shamu, G. F. Auchampaugh, N. S. P. King, M. S. Moore, G. L. Morgan, and T. S. Singleton, Phys. Rev. Lett. **49**, 255 (1982).

[31] A. J. Koning and J. P. Delaroche, Nucl. Phys. **A713**, 231 (2003).

[32] C. Y. Chih and W. M. Powell, Phys. Rev. **106**, 539 (1957).

[33] T. C. Griffith, A. P. Banford, M. Y. Uppal, and W. S. C. Williams, Proc. Phys. Soc. **71**, 305 (1958).

[34] A. J. Bersbach, R. E. Mischke, and T. J. Devlin, Phys. Rev. D **13**, 535 (1976).

[35] J. P. Scanlon, G. H. Stafford, J. J. Thresher, P. H. Bowen, and A. Langsford, Nucl. Phys. **41**, 401 (1963).

[36] R. A. Arndt, I. I. Strakovsky, and R. L. Workman, Phys. Rev. C **62**, 034005 (2000).

[37] V. G. J. Stoks, R. A. M. Klomp, C. P. F. Terheggen, J. J. de Swart, Phys. Rev. C **49**, 2950 (1994).

[38] R. Machleidt, Adv. Nucl. Phys. **19**, 189 (1989).

[39] R. Machleidt, Phys. Rev. C **63**, 024001 (2001).

[40] M. Lacombe, B. Loiseau, J. M. Richard, R. Vinh Mau, J. Côté, P. Pirèls, and R. de Tourreil, Phys. Rev. C **21**, 861 (1980).

[41] G. C. Wick, Atti R. Accad. Naz. Lincei, Mem. Cl. Sci. Fis. Mat. Nat. **13**, 1203 (1943).

[42] G. C. Wick, Phys. Rev. **75**, 1459 (1949).

[43] G. R. Satchler, *Introduction to Nuclear Reactions* (Macmillan Education Ltd., Oxford, 1990), p. 118.

[44] T. Peterson *et al.*, Nucl. Phys. **A663-664**, 1057c (2000).

[45] M. Sarsour *et al.* (submitted for publication to Phys. Rev. Lett.).